

CO₂ packing polymorphism under confinement in cylindrical nanopores

Ilaria Gimondi¹ and Matteo Salvalaglio^{1, a)}

Thomas Young Centre and Department of Chemical Engineering, University College London, London WC1E 7JE, UK.

(Dated: 12 November 2018)

We investigate the effect of cylindrical nano-confinement on the phase behaviour of a rigid model of carbon dioxide using both molecular dynamics and well tempered metadynamics. To this aim we study a simplified pore model across a parameter space comprising pore diameter, CO₂-pore wall potential and CO₂ density. In order to systematically identify ordering events within the pore model we devise a generally applicable approach based on the analysis of the distribution of intermolecular orientations. Our simulations suggest that, while confinement in nano-pores inhibits the formation of known crystal structures, it induces a remarkable variety of ordered packings unrelated to their bulk counterparts, and favours the establishment of short range order in the fluid phase. We summarise our findings by proposing a qualitative phase diagram for this model.

Keywords: polymorphism, carbon dioxide, confinement, metadynamics, phase diagram

I. INTRODUCTION

Confinement is known to play a role in the phase behaviour of molecular solids, most notably affecting polymorph selection^{1,2}. For instance, a paradigmatic example of the dramatic effects of confinement on the spatial arrangement of molecules is provided by water, which, as proven both experimentally and computationally, displays a counter-intuitively complex phase diagram under confinement³⁻¹⁰. Understanding polymorphism in confined volumes is relevant both to describe natural processes^{11,12} as well as for driving rational materials and process development^{13,14}. Despite its importance a systematic understanding of confinement effects is still lacking.

Following up a recent work, in which we have investigated the thermodynamics and mechanism of phase transition between CO₂ forms I and III in bulk, we set out to study the effect of confinement on CO₂ condensed phases. We tackle this problem by carrying out a systematic analysis of CO₂ phase behaviour confined in weakly interacting cylindrical nano pores. Our work has a two-fold aim: on the one hand understanding phase behaviour of confined CO₂ is relevant due to its prominent role within the carbon cycle, and the surging needs for mitigating its emissions in atmosphere by implementing capture and storage technologies based on adsorption in porous solids¹⁵⁻¹⁸. On the other hand due to its modest structural complexity accompanied with a rich phase diagram, CO₂ represents a convenient model system to perform extensive sampling of polymorphic transitions at finite temperature¹⁹ and gain insight on general aspects of molecular phase transitions under confinement.

Both experiments and theory highlight remarkable effects of confinements on CO₂ phase behavior. For instance, the density of confined CO₂ can significantly exceed the fluid phase bulk density²⁰⁻²⁵ reaching val-

ues comparable to that of solid CO₂ and displaying signs of orientational correlations and structural rearrangements^{20,21}.

Several examples of molecular modelling studies can be found investigating the transport of CO₂ in a confined fluid phase^{24,26,27}, and the modelling literature characterising structural features of CO₂ under confinement is limited. An insightful work from Elola and Rodriguez has recently proposed a detailed analysis of the CO₂ fluid structure within silica pores, highlighting how confinement induces a layered arrangement in the fluid phase and determines a significant slowdown of both translational and rotational diffusion of CO₂ molecules²⁵.

In our work we aim complementing the state of the art by understanding whether confinement promotes or inhibits the formation of ordered phases. To this aim we systematically analyse the intermolecular structural organisation of CO₂ confined in a simplified pore geometry consisting of a cylinder of Lennard-Jones (LJ) particles. We carry out a systematic study as a function of the cylinder radius (spanning from 1 to 5 nm), the nominal density of CO₂ molecules (5 - 15 molecules/nm³), and the interaction potential with the pore walls. We investigate this parameter space by systematically carrying out unbiased molecular dynamics simulations starting from liquid-like initial conditions, and by enhancing the exploration of ordered molecular packings with metadynamics.

Our analysis shows that, while the formation of known solid CO₂ arrangements is inhibited, confinement unveils a rather complex behaviour. Depending on the location in parameter space, confined CO₂ can either approach a completely disordered fluid state, exhibit short-range orientation correlations or arrange into long-range ordered packings. By systematically analysing relative orientations distributions we have systematically detected ordering events from molecular trajectories and classified ordered configurations.

This paper is organized as follows: firstly, in section 2, we introduce the model system, methods, parameters space, and the analysis tools developed to characterise ordering transitions. In section 3 we present and discuss

^{a)}Electronic mail: m.salvalaglio@ucl.ac.uk

our results, and finally in section 4 we summarise our findings by proposing a qualitative phase diagram in the space defined the nominal density of the pore and its normalised radius.

II. METHODS

To investigate the effect of confinement on liquid carbon dioxide we have employed both standard molecular dynamics (MD)^{28–30} and well-tempered metadynamics (WTMetaD)³¹. For a detailed description of metadynamics we refer to Barducci et al.^{31,32}, and Valsson et al.³³, and for a brief overview of its applications in crystallisation studies to Giberti et al.³⁴. In the following we report the setup of the molecular model investigated, the details of MD simulations and WTmetaD simulations setup, and the analysis approach implemented to detect and characterise the emergence of an ordered phase from an initial liquid state.

CO₂ Potential. In order to model CO₂ we employ the Transferable Potentials for Phase Equilibria (TraPPE) force field^{35,36} (Table I) with the introduction of dummy atoms to maintain molecules rigid with a 180° angle without inducing instability²⁴. This choice is consistent with our previous work on carbon dioxide polymorphism at high pressure¹⁹, and allows for a direct comparison with results obtained in bulk.

TABLE I. Parameters for the TraPPE force field

m_C	m_O	σ_{C-C}	σ_{O-O}	ϵ_{C-C}
		[nm]	[nm]	[kJ/mol]
12	16	0.280	0.305	0.224
ϵ_{O-O}	q_c	q_o	l_{C-O}	α_{O-C-O}
[kJ/mol]	[e]	[e]	[Å]	[°]
0.657	0.70	-0.35	1.160	180

Pore Model. To develop a simplified model to study confinement in a weakly interacting porous medium, we build a single-wall cylindrical nanopore of LJ particles. We consider different pore diameters (1, 1.3, 2, 5 nm) with a constant wall density of 33.104 atoms/nm² and a height of 10 nm for all diameters except the case with diameter 5 nm, where the height has been limited to 5 nm as well for the sake of computational efficiency. The cylinder axis aligns with z . We also investigate the effect induced by variations in the wall potential induced by keeping constant ϵ_{wall} while varying the σ_{wall} , in the interval between 0.253 to 0.405 nm.

Simulation set up. For our simulations we choose temperature conditions of 323 K and nominal carbon dioxide densities compatible with supercritical CO₂^{18,22,24}. Firstly, we run NVT molecular dynamics simulations of the described system, with Bussi-Donadio-Parrinello³⁷ thermostat. We apply periodic boundary conditions (*pb*c) to ensure continuity along z , i.e. the

cylinder axis. To avoid overlapping effects in the radial direction from periodic images, the simulation box is much larger (around 10 times) than the pore diameter. Lennard-Jones potential with Lorentz-Berthelot combination rules and long-range corrections is employed. Typical MD simulations are 20 ns-long, starting from disordered configurations equilibrated for 100 ps.

We use the same setup to carry out WTMetaD simulations aimed at exploring the space of accessible packings beyond the timescale limit of unbiased MD. As collective variable we employ an order parameter, hereafter indicated with λ , that expresses the degree of crystallinity of a system based on the local environment around each molecule. A complete description of the mathematical formulation of λ has been reported by Giberti et al.³⁸. Explorative WTMetaD simulations are carried out biasing two distinct formulations of the λ order parameter: λ_I , tuned to capture the molecular arrangement of CO₂ form I, which we recently developed to investigate CO₂ polymorphism at high pressure¹⁹; and λ_B , based instead on the characteristic angles and local density of the most abundant ordered structure observed under confinement (configuration B in Table IV). For details on the parameters used to define both λ_I and λ_B refer to Table II. Further details about the WTMetaD set up are reported in the Supporting Information.

TABLE II. Tuning of the λ -order parameters. The table reports θ_1 , its supplementary θ_2 , the associated width of the Gaussian, δ , which for symmetry reasons is the same for both angles. The cut-off values for the number of neighbours and the coordination shell are presented as well.

	θ_1 [°]	θ_2 [°]	$\delta_1 = \delta_2$ [°]	n_{cut} [-]	r_{cut} [Å]
λ_I	70.47	108.86	14.32	5	4
λ_B	46.18	133.82	5.21	3	4

Parameter space representation. In order to represent our results throughout parameter space in a rational and efficient form we define a single adimensional radius, r' , which accounts for variations in both LJ potential (σ_{wall}) and pore size and quantifies the void space available within the pore⁵. The adimensional radius r' is defined by the following expression:

$$r' = \frac{r_{pore} - \sigma_{m,C-wall}}{\sigma_{m,C-C}} \quad (1)$$

where $\sigma_{m,C-wall}$ represents the distance from the wall to the minimum of the C-wall potential (as in Figure 1(a), for $\sigma_{wall} = 0.34$ nm) and $\sigma_{m,C-C}$ is the position of the minimum of the C-C interaction. Values of r' for all simulations performed in this work are reported in Table III. The second parameter is the nominal density of CO₂ molecules within the pore ρ_{CO_2} , computed accounting for the volume of the cylinder of diameter d_{pore} .

Systematic detection of ordered arrangements. In the definition of ordered parameters such as λ the identification of characteristic relative orientations is key^{19,34,39}.

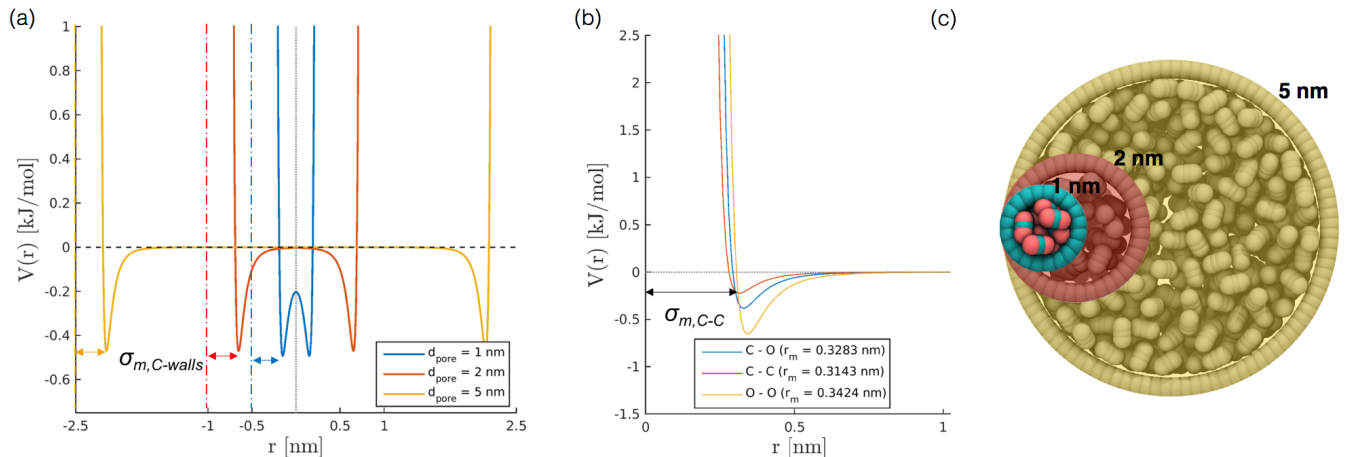


FIG. 1. Simulations setup. (a) Representation of the LJ potential for the interaction between the pore wall and the carbon atom of CO_2 we report three pore sizes ($d_{\text{pore}} = 1, 2, 5$ nm), for which the zero on the x axis represents the cylinder axis and the walls are located at $\pm 0.5, \pm 1$ and ± 2.5 nm, respectively; σ_{wall} is set to 0.34 nm. Arrows highlight $\sigma_{m,C\text{-wall}}$ (b) Intermolecular LJ potential characterising CC, CO and OO non bonded interactions. The x axis represents the interatomic distance; the black arrow indicates $\sigma_{m,C-C}$. (c) Representation of the cross-section of the initial configuration for simulations with $d_{\text{pore}} = 1, 2$, and 5 nm.

This is typically based on the analysis of the distribution of relative orientations that characterises a relevant structure, as extensively discussed for bulk CO_2 in Ref. ¹⁹. Indeed the relative orientation between molecular axes of neighbouring molecules represents a *fingerprint* of each arrangement and in principle allows to distinguish not only between liquid and solid, but also among different solid structures. An example of such distributions for bulk dry ice and liquid CO_2 is reported in Figure 2. In the following we build on this observation to systematically detect ordering phenomena in within molecular trajectories.

As reported in Figure 2, crystal and liquid carbon

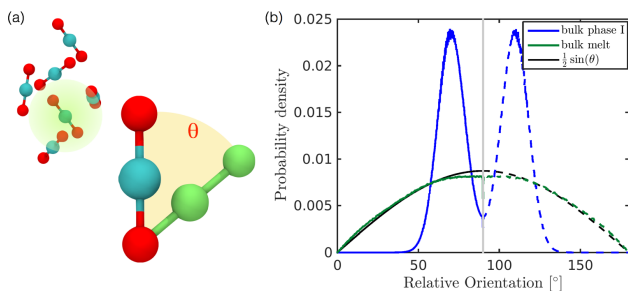


FIG. 2. (a) The distribution of relative orientations is built considering all the angles between an assigned molecule and its nearest neighbours, falling within a sphere of radius r_{cut} represented in transparent green. The relative orientation is computed as the elevation angle between the axis of two CO_2 molecules. (b) Characteristic angle distribution for bulk phases, in particular melt (green) and phase I (blue); the analytical expression for the random distribution in melt is also reported in black.

TABLE III. Value of r' for the combinations of d_{pore} and σ_{wall} investigated.

r'	d_{pore} [nm]			
	1	1.3	2	5
0.253	0.639	1.116	2.230	7.003
0.315	0.528	1.006	2.119	6.892
σ_{wall} [nm] 0.340	0.484	0.961	2.075	6.847
0.372	0.427	0.904	2.017	6.790
0.405	0.368	0.845	1.959	6.731

dioxide display significantly different characteristic orientation distributions. In order to quantitatively capture such difference we apply the Bhattacharyya distance⁴⁰, a metric that quantifies the *dissimilarity* of two probability densities. The Bhattacharyya distance D_B between two angle distributions $p(\theta)$ and $q(\theta)$ is defined as:

$$D_B(p, q) = -\ln(C_B(p, q)) \quad (2)$$

where C_B is the Bhattacharyya coefficient, which measures the overlap between $p(\theta)$ and $q(\theta)$ defined as:

$$C_B(p, q) = \int \sqrt{p(\theta)q(\theta)} d\theta \quad (3)$$

In our analysis we take advantage of the fact that a completely random arrangement of linear molecules displays a relative orientation probability density characterised by the functional form $p_{\text{ref}} = 1/2 \sin \theta$. For a derivation of the reference distribution functional form see the Supporting Information. As shown in Figure 2 the distribution of angles in the bulk of liquid CO_2 closely resembles the theoretical random distribution p_{ref} .

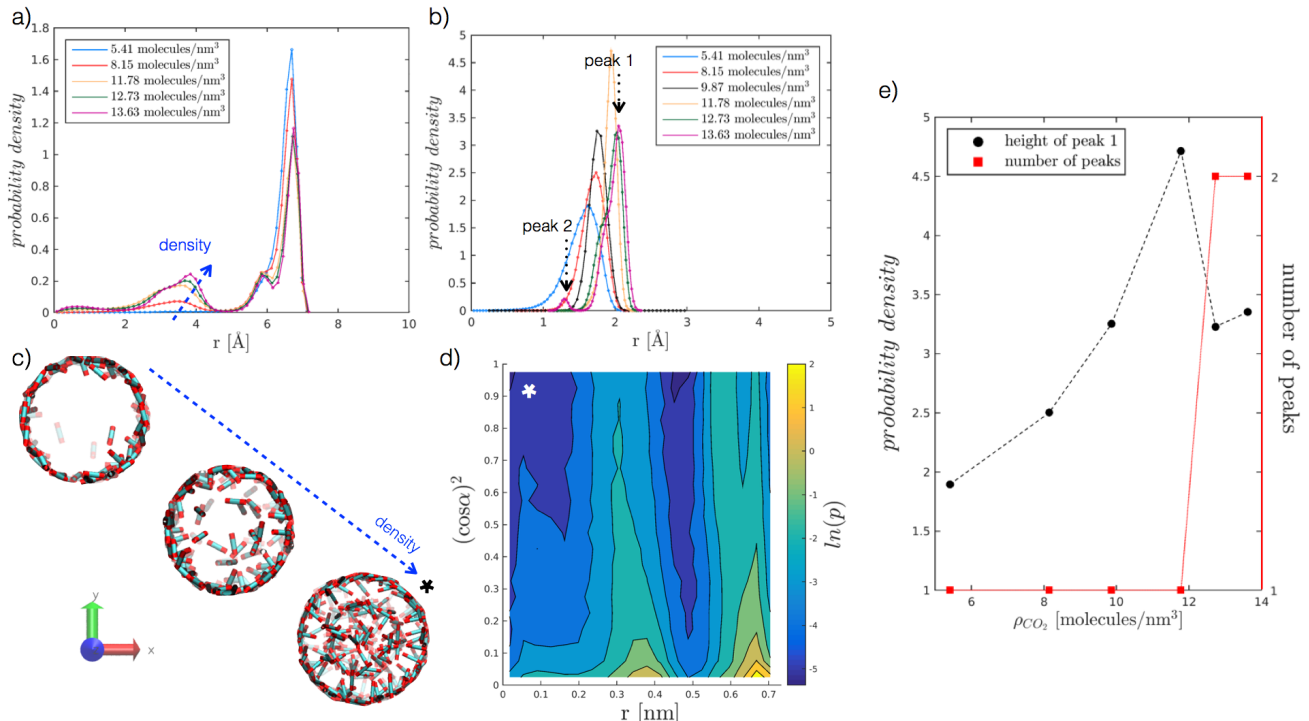


FIG. 3. Probability density profiles associated with the position of CO_2 molecules in the radial direction of the pore, for the range of densities investigated at different values of r' . In particular, (a) refers to $r' = 2.075$, and (b) to $r' = 0.484$. Along the abscissa, i.e. the pore radius, zero corresponds to the cylinder axis, while the maximum value reported to the radius of the pore. For the case in (b), (e) further analyses the height of the adsorbed layer peak and the number of peaks as a function of ρ_{CO_2} . For the case in (a), instead, (c) reports snapshots of hollow to filled structures for increasing ρ_{CO_2} , from 5.41 to 8.15 to 12.73 molecules/ nm^3 . More in detail, (d) presents the probability density of the angle α as a function of the radial distance, for $r' = 2.075$ and $\rho_{\text{CO}_2} = 12.73$ molecules/ nm^3 . The angle α , reported as $(\cos\alpha)^2$, is evaluated between CO_2 molecular axis and the vector normal to the pore walls; to enhance the differences on the plot the probability density is represented by its logarithm. The x -axis convention is the same as before, with cylinder axis in zero.

Given a molecular trajectory, we can therefore define a time dependent measure of the deviation from an ideal random packing of CO_2 molecules as:

$$D_B(t) = -\ln \int \sqrt{\frac{1}{2}p(\theta, t)} \sin\theta d\theta \quad (4)$$

where $p(\theta, t)$ is the instantaneous probability density of relative orientations.

The construction of $p(\theta, t)$ is straightforward for carbon dioxide, due to its linear, symmetrical geometry. For each molecule we evaluate the polar angle between its molecular axis and the analogous vector in each one of its nearest neighbours, i.e. molecules within a cut-off radius of 4 Å for ordered phases and 5 Å for the liquid as shown in Figure 2(a).

Tools. Pores are built using an in-house FORTRAN code, while we use Packmol⁴¹ to insert carbon dioxide molecules at random positions and orientations in order to avoid any creation of patterns. For MD and WTMetaD simulations we employ Gromacs 5.2.1⁴² and Plumed 2.2⁴³. Post-processing of the results is carried on with MATLAB (R2015a), Visual Molecular Dynamics (VMD)⁴⁴ and Plumed 2.2⁴³.

III. RESULTS AND DISCUSSION

In this section we present and discuss the results of our molecular dynamics investigation of the effect of confinement on CO_2 ordering. Preliminary simulations were carried out to investigate the equilibrium distribution of a single CO_2 molecule in the presence of a cylindrical LJ wall and are discussed in Supporting Information. In the following we begin by discussing the arrangement of CO_2 molecules within the pore as a function of pore size and density, and we continue by reporting an analysis of the ordered arrangements identified within our parameter space.

Molecular arrangement within the pore. We begin by analysing the arrangement of CO_2 molecules in the pores at increasing ρ_{CO_2} . In the case of low densities we observe the formation of a single layer of adsorbed CO_2 molecules in contact with the pore surface associated with a hollow structure. With increasing ρ_{CO_2} larger pores ($d_{\text{pore}} = 2$ and 5 nm), can accommodate a second layer of CO_2 , and then display bulk-like filling as shown in Figure 3(a,c). This finding is in agreement with the results obtained by Erola and Rodriguez²⁵ for CO_2 confined in silica pores.

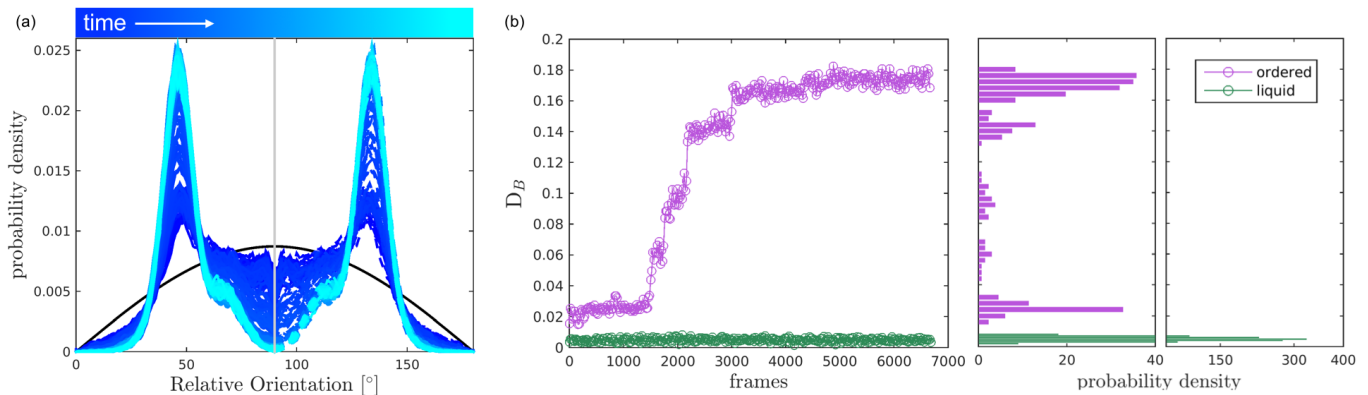


FIG. 4. Bhattacharyya analysis of an ordering phenomenon. (a) Temporal evolution of the angle distribution, $p(\theta, t)$, for $r' = 0.484 - \rho_{CO_2} = 11.78$ molecules/nm³, where colour dark blue to light blue represents time increment, while the black distribution is the probability density for melt, employed as reference p_{ref} for evaluating D_B . (b) Bhattacharyya distance, D_B , as a function of time for an example of ordering (violet, $r' - \rho_{CO_2}$ as (a)) and fluid (green, $r' = 0.961 - \rho_{CO_2} = 5.41$ molecules/nm³ conditions; the probability density of D_B is also reported in the form of a histogram.

Furthermore, we analyse CO₂ molecular orientation within the pore by evaluating the angle α between the molecular axis and the normal to the pore surface. As shown in Figure 3 (d), we can clearly note the high probability regions in the $r, (\cos \alpha)^2$ plane, corresponding to individual layers. We note that in both layers α is narrowly distributed around 90°. This indicates that CO₂ molecules arrange parallel to the pore surface, in agreement with observations reported in the literature^{21,24,25,45}.

In smaller pores ($d_{pore} = 1$ and 1.3 nm) a layered structure is not observed and the decrease in height of the dominant peak (peak 1 in Figure 3(b)), accompanied by the appearance of a secondary peak (peak 2 in Figure 3(b)) is instead associated with a reorganisation of the CO₂ packing within the pore (see Figure 3(b,e)). For instance, we note that at $d_{pore} = 1.3$ nm, CO₂ arranges as a chain along the z axis for densities equal or above 9.87 molecules/nm³.

Detecting emerging order. After discussing the position and alignment of CO₂ molecules with respect to the pore wall, we delve into the analysis of intermolecular arrangement. In particular, we analyse the arrangement of the local environment around each CO₂ molecule by monitoring the distribution of relative orientations. As mentioned in section 2, this information constitutes a structural *fingerprint* and can discriminate not only between ordered and disordered arrangements but also among different ordered packings.

As discussed in section 2, to detect the unfolding of ordering events we compute the Bhattacharyya distance, $D_B(t)$ with respect to an ideal random packing for each MD trajectory. When ordered arrangements nucleate within a pore, the D_B metric displays a sharp increase. An example of this behaviour in a typical trajectory is reported in Figure 4, where in (b) we compare the trend of $D_B(t)$ for a trajectory undergoing an ordering transi-

tion (violet) and a trajectory that remains stable in the fluid state (green). In Figure 4(a) the evolution of the instantaneous intermolecular angle distribution $p(\theta, t)$ is reported together with the $p_{ref}(\theta)$ corresponding to an ideal random packing.

Mapping phase behaviour in the (ρ_{CO_2}, r') parameter space. The systematic analysis of the deviation from an ideal random packing and the contextual detection of the appearance of ordered phases from a liquid configuration allows to clearly map the qualitative behaviour of confined CO₂ within the (ρ_{CO_2}, r') parameter space. In particular we can identify areas where CO₂ under confinement spontaneously evolves to ordered packings within the characteristic timescale of in MD simulations. To further analyse our finding, we complement the analysis of the angle distribution by reporting the C-C radial pair distribution function $g(r)$. Inspecting both $g(r)$ and relative orientation distribution we can identify three regions in parameter space: a disordered region (Figure 5 green area, examples (a-b)), an ordered region (Figure 5 violet area, examples (e-f)), and a transition region between them (Figure 5 green-to-violet area, examples (c-d)). We note that in the disordered region, at large r' and low density, the distribution of relative orientations approaches the ideal random distribution and the $g(r)$ displays the short-range order typical of a liquid. On the contrary, in the ordered region both the angle distribution and the $g(r)$, deviate from the typical liquid behaviour denoting long-range order through the presence of characteristic peaks in both orientation distribution and $g(r)$. Finally, the transition region denotes a peculiar behaviour. In this region of parameter space, while $g(r)$ maintains a close resemblance to that of a liquid phase, the distribution of relative orientations displays significant deviations from an ideal random packing suggesting the development of correlation in the relative orientation of CO₂ molecules.

From the analysis of the transitions obtained in the

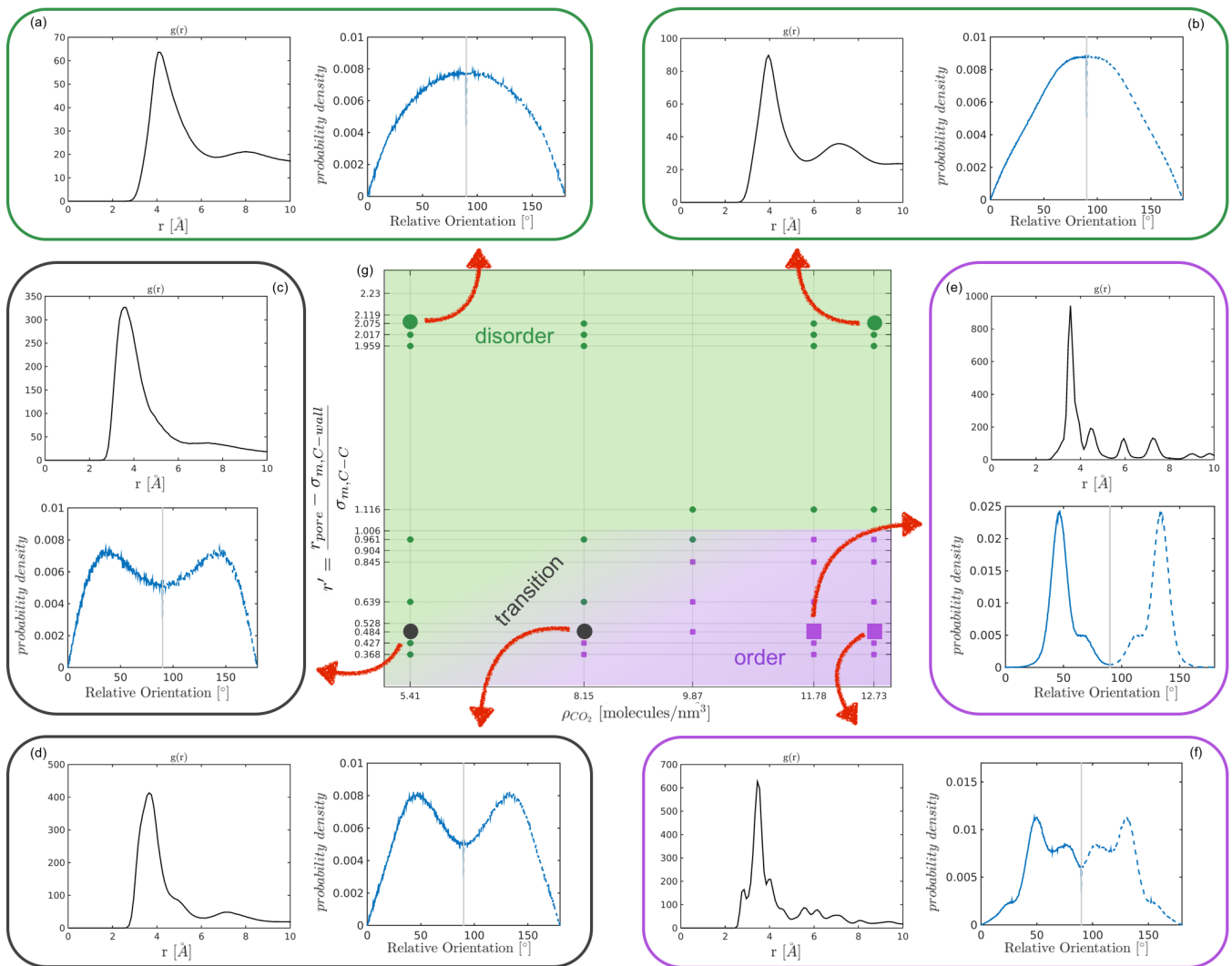


FIG. 5. Radial pair distribution function, $g(r)$ (black) and angle distribution (blue) for illustrative cases of liquid (a-b), transition (c-d), and ordered structures (e-f). In particular, (a) refers to $r' = 2.075 - \rho_{CO_2} = 5.41$ molecules/nm³, (b) to $r' = 2.075 - \rho_{CO_2} = 12.73$ molecules/nm³, (c) to $r' = 0.484 - \rho_{CO_2} = 5.41$ molecules/nm³, (d) to $r' = 0.484 - \rho_{CO_2} = 8.15$ molecules/nm³, (e) to $r' = 0.484 - \rho_{CO_2} = 11.78$ molecules/nm³, and (f) to $r' = 0.484 - \rho_{CO_2} = 12.73$ molecules/nm³. Green areas on the phase diagram refer to fluid state, violet to ordered, while violet-to-green colour to transition structures

structured region of parameter space we notice a finer grained level of complexity emerging. As displayed by the qualitative comparison of both the distribution of relative orientations and the $g(r)$ reported in examples Figure 5(e) and (f) multiple ordered packings can be obtained.

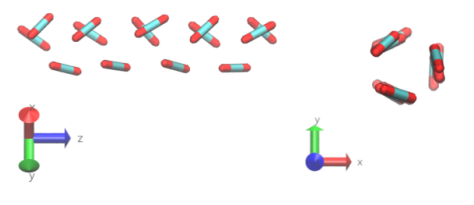
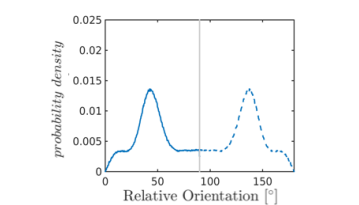
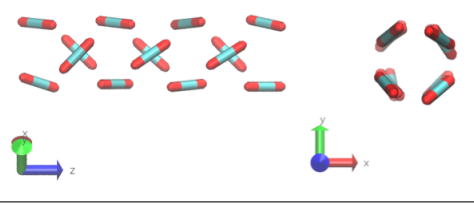
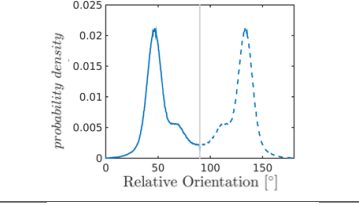
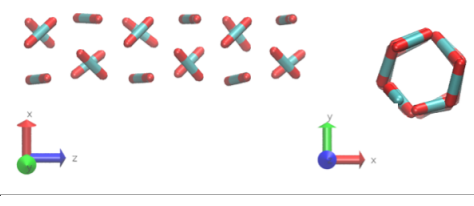
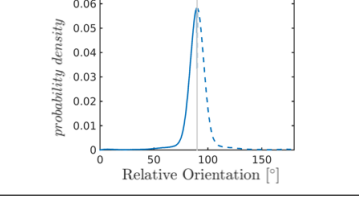
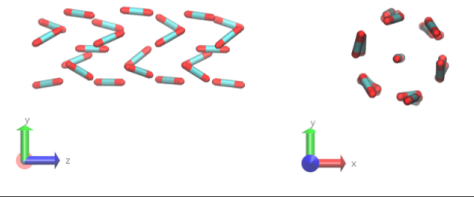
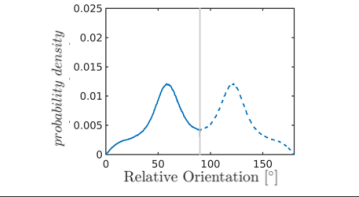
Stable ordered packings. We now move on to present a detailed analysis of the ordered structures encountered within the ordered region of the (ρ_{CO_2}, r') phase diagram. We shall note that, in order to confirm the finding emerging from unbiased simulations, we have applied WTMetaD simulations to further sample the configuration space of confined CO₂. This allows to verify that in the disordered or transition regions ordered arrangements cannot be found or, when found do not states with a finite lifetime and spontaneously revert to liquid in un-

biased MD.

Nevertheless, in the region of the phase diagram where confinement-induced order emerges, we identify four different stable arrangements. We assign to such arrangements a label progressing from A to D, based on their structural features. As we can see in Table IV, progressing from A to D these structures present an increasing number of molecules in their repeating unit. Moreover, the same classification applies when analysing the geometry of the apparent ring that characterises the horizontal cross-section of the pore (see Table IV). The number of ring members is 3 in A, 4 in B, and 6 in both C and D, with D displaying one molecule in the middle of the pore oriented parallel to the pore longitudinal axis.

As far as the packing of these four ordered structures is concerned, it can be seen that the characteristic angle dis-

TABLE IV. Molecular representation of the arrangement and characteristic angles distribution for the ordered structures identified. Such structures are named A to D according to the apparent number of ring members when observed from the top. The angles distributions are obtained at $\Gamma = 0.484 - \rho_{CO_2} = 9.87$, at $r' = 0.484 - \rho_{CO_2} = 11.78$, at $r' = 0.484 - \rho_{CO_2} = 12.73$, at $r' = 0.961 - \rho_{CO_2} = 12.73$, for A, B, C, and D, respectively.

Label	Snapshots	Relative Orientation Distribution
A		
B		
C		
D		

tribution represents a clear fingerprint of their molecular arrangement (Table IV), while the coordination number appears to be a function of the total density inside the pore and cannot clearly discriminate between different arrangements. In particular, the orientation distribution of B presents well-defined peaks in $\theta_1 = 46.2^\circ$ and symmetrically in $\theta_2 = 133.8^\circ$, while C a very sharp single one in $\theta = 90^\circ$. Structure A, instead, appears to be an intermediate between B and C both from the inspection of the coordinates and from its characteristic angle distribution. Indeed, while the most densely populated orientations closely resemble those of B, the peak at 90° is more pronounced than in B. Form D present instead wider peaks in $\theta_1 = 57.9^\circ$ and the additional peak $\theta_2 = 122.1^\circ$.

Interestingly, three out of four ordered structures, more precisely A, B, and D, form spontaneously in unbiased MD simulations; phase C, instead, is generated from metadynamics simulations performed in conditions that spontaneously yielded other ordered arrangements (vio-

let area in the r'/ρ_{CO_2} phase diagram in Figures 5 and 6); structure C is confirmed to be a metastable state for the system possessing a finite lifetime through 20 ns long unbiased MD simulations, initialised in configuration C, which do not display any sign of instability transition. It should be noted that the exploration carried out with WTMetaD yields additional ordered arrangements, which, however, do not survive unbiased MD and are therefore considered to be unstable (see SI).

In addition metadynamics further confirms that for ρ_{CO_2} - r' conditions that induce spontaneous ordering, the disordered liquid state is strongly disfavoured with respect to the ordered phases. Indeed even in extended WTMetaD simulations, characterised by the deposition of significant bias, no melting event can be observed, while transitions between ordered arrangements are routinely detected. This finding is consistent irrespective of the set of CVs used to enhance the exploration and suggests that the energetic barrier associated with melting is higher than the barriers associated with solid-solid

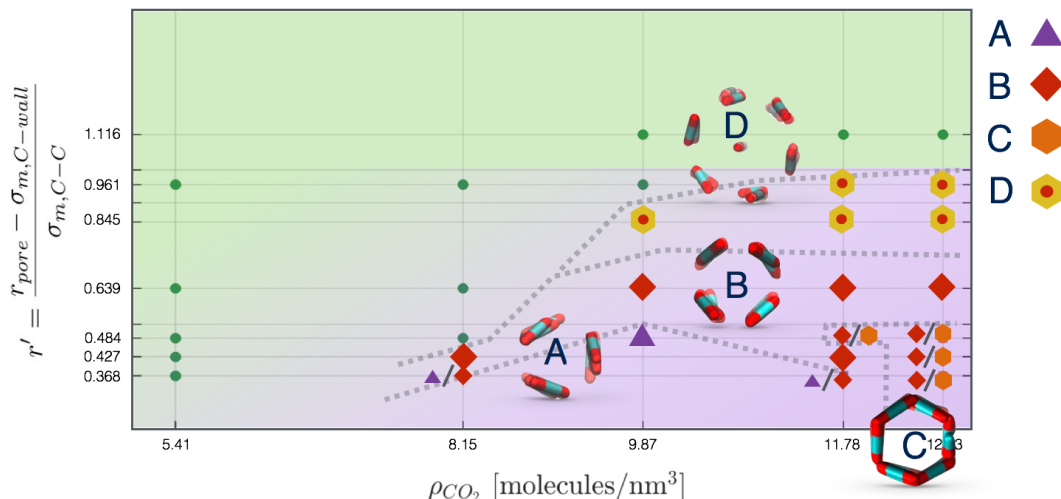


FIG. 6. Qualitative phase diagram of CO_2 confined in weakly attractive cylindrical nanopores. In green is represented the region of phase space characterised by disordered configurations, while we report in violet the region of phase space where ordered structures are found. Configurations yielding one or more amongst packing A, B, C, and D are appropriately marked. Qualitative phase boundaries have been reported in order to highlight how simulations yielding similar structures tend to cluster in parameter space, suggesting that the spontaneous ordering process observed from MD reflects the underlying thermodynamic stability of the packings.

interconversion.

Furthermore, the conversion from hollow (A, B, C) to filled (D) ordered structures and vice versa is not sampled during WTMetaD simulations; this transition appears unlikely in the conditions investigated since, as discussed before, different values of r' can accommodate different numbers of CO_2 layers.

On the other hand, transition between phase A, B and C is possible and consistently sampled. More precisely, it takes place through a gradual reorganisation of the layers that starts in a localised region and then spreads through the entire pore length. Interestingly, WTMetaD allows to sample mixed arrangements of different packings, (e.g. half ordered as B and half as C) which reveal to be stable in subsequent MD simulation, confirming that solid-solid interconversion is an activated event. Moreover, in these structures it is common to find boundary regions in which the order is not well-defined, effectively acting as defects within the pore.

IV. CONCLUSIONS

In this work we present a systematic investigation of the effects of confinement in cylindrical nanopores on CO_2 , as a function of pore size, wall potential and CO_2 density. To systematically detect the formation of ordered packings we have devised a general analysis approach based on the calculation of the time-dependent Bhattacharyya distance between a reference probability density and the instantaneous probability density of the relative orientation of nearest neighbours. Here we have

adopted as a reference an ideal random packing, which closely approximates the distribution of relative orientations in the bulk of the liquid phase. This analysis approach is general and we anticipate its applicability to a much wider range of phase transitions in molecular solids.

We find that cylindrical confinement induces polymorph selection by inhibiting the nucleation of known solid forms of CO_2 while at the same time inducing the organisation of CO_2 into a series of distinct ordered arrangements, which do not resemble any of the known CO_2 polymorphs. Using a combination of unbiased MD and WTMetaD we identify four ordered packing that are stable in the region of parameter space corresponding to small pore radii and large densities. These configurations have been labelled A, B, C and D following the progression in the number of CO_2 molecules visible in a cross-section of a pore. Interestingly, none of these configurations corresponds to known bulk structures. It should be noted that, while A, B, and D emerge spontaneously from unbiased MD, C is found from the enhanced exploration of the configuration space achieved with WTmetaD.

In Figure 6 we report a qualitative phase diagram that summarizes the identified structures and the regions of parameter space where such structures have obtained. Markers point the location in parameter space where specific packings have been observed. Cases in which multiple configurations are indicated on the phase diagram represent points in which multiple arrangements have been observed either with unbiased MD or through WTMetaD. We observe that, in the ordered region of the phase diagram WTMetaD was quite efficient in promot-

ing transitions between ordered packings, however it was unable to induce melting. Despite its qualitative character, this observation suggests that within the ordered region of the phase diagram solid-solid interconversion is energetically favoured with respect to liquid mediated transitions.

Finally we observe that, even in the disordered region confinement induces a short-range organisation of the liquid phase, in which the distribution of relative orientations departs from an ideal random packing, as shown in Figure 5. At large volumes and low densities the bulk behaviour is recovered as expected.

To conclude we note how such a simple model system such as CO₂ confined in a simple nanometric pore model unveils remarkable structural complexity, showcasing the profound effect of confinement on the phase behaviour of molecular solids. This work paves the way for a systematic assessment of CO₂ packing polymorphism in systems characterised by realistic pore geometries and surface chemistry.

CONFLICT OF INTEREST

There are no conflicts to declare.

ACKNOWLEDGEMENTS

The authors acknowledge EPSRC (Engineering and Physical Sciences Research Council) for PhD scholarship, and UCL Legion High Performance Computing Facility for access to Legion@UCL and associated support services, in the completion of this work.

SUPPLEMENTARY MATERIAL

See supplementary material for single molecule probability distribution in the model pore, derivation of the ideal random distribution $p_{ref}(\theta)$, details of the setup and results of explorative metadynamics simulations, additional analysis of the radial density profiles. .

REFERENCES

- Jeong-Myeong Ha, Johanna H. Wolf, Marc A. Hillmyer, and Michael D. Ward. Polymorph selectivity under nanoscopic confinement. *J. Am. Chem. Soc.*, 126(11):3382–3383, 2004. PMID: 15025439.
- Antonio Llins and Jonathan M. Goodman. Polymorph control: past, present and future. *Drug Discov. Today*, 13(5):198 – 210, 2008.
- Yutaka Maniwa, Hiromichi Kataura, Masatoshi Abe, Shinzo Suzuki, Yohji Achiba, Hiroshi Kira, and Kazuyuki Matsuda. Phase Transition in Confined Water Inside Carbon Nanotubes. *J. Phys. Soc. Jpn.*, 71(12):2863–2866, dec 2002.
- A. Striolo, A. A. Chialvo, K. E. Gubbins, and P. T. Cummings. Water in carbon nanotubes: Adsorption isotherms and thermodynamic properties from molecular simulation. *J. Chem. Phys.*, 122(23):234712, jun 2005.
- Haruka Kyakuno, Kazuyuki Matsuda, Hitomi Yahiro, Yu Inami, Tomoko Fukuoka, Yasumitsu Miyata, Kazuhiro Yanagi, Yutaka Maniwa, Hiromichi Kataura, Takeshi Saito, Motoo Yumura, and Sumio Iijima. Confined water inside single-walled carbon nanotubes: Global phase diagram and effect of finite length. *J. Chem. Phys.*, 134(24):244501, jun 2011.
- G Algara-Siller, O Lehtinen, F C Wang, R R Nair, U Kaiser, H a Wu, a K Geim, and I V Grigorieva. Square ice in graphene nanocapillaries. *Nature*, 519(7544):443–5, 2015.
- Alan K. Soper. Physical chemistry: Square ice in a graphene sandwich. *Nature*, 519(7544):417–418, mar 2015.
- Kumar Varoon Agrawal, Steven Shimizu, Lee W. Drahushuk, Daniel Kilcoyne, and Michael S. Strano. Observation of extreme phase transition temperatures of water confined inside isolated carbon nanotubes. *Nat. Nanotechnol.*, 12(3):267–273, nov 2016.
- Ji Chen, Georg Schusteritsch, Chris J. Pickard, Christoph G. Salzmann, and Angelos Michaelides. Two Dimensional Ice from First Principles: Structures and Phase Transitions. *Phys. Rev. Lett.*, 116(2):025501, jan 2016.
- Ji Chen, Andrea Zen, Jan Gerit Brandenburg, Dario Alfè, and Angelos Michaelides. Evidence for stable square ice from quantum Monte Carlo. *Phys. Rev. B*, 94(22):220102, dec 2016.
- Christopher J. Stephens, Sophie F. Ladden, Fiona C. Meldrum, and Hugo K. Christenson. Amorphous calcium carbonate is stabilized in confinement. *Adv. Funct. Mater.*, 20(13):2108–2115, 2010.
- Yun-Wei Wang, Hugo K. Christenson, and Fiona C. Meldrum. Confinement leads to control over calcium sulfate polymorph. *Adv. Funct. Mater.*, 23(45):5615–5623, 2013.
- Alfred Y. Lee, In Sung Lee, Severine S. Dette, Jana Boerner, and Allan S. Myerson. Crystallization on confined engineered surfaces: a method to control crystal size and generate different polymorphs. *J. Am. Chem. Soc.*, 127(43):14982–14983, 2005. PMID: 16248610.
- M. Beiner, Rengarajan, S. Pankaj, D. Enke, and M. Steinhart. Manipulating the crystalline state of pharmaceuticals by nanoconfinement. *Nano Lett.*, 7(5):1381–1385, 2007. PMID: 17439189.
- Sally M. Benson. Overview of Geologic Storage of CO₂. In *Carbon Dioxide Capture for Storage in Deep Geologic Formations*, volume 2, pages 665–672. Elsevier, 2005.
- F M Orr. Onshore Geologic Storage of CO₂. *Science*, 325(5948):1656–1658, sep 2009.
- Niall MacDowell, Nick Florin, Antoine Buchard, Jason Hallett, Amparo Galindo, George Jackson, Claire S Adjiman, Charlotte K Williams, Nilay Shah, and Paul Fennell. An overview of co 2 capture technologies. *Energ. Environ. Sci.*, 3(11):1645–1669, 2010.
- Samuel Krevor, Martin J. Blunt, Sally M. Benson, Christopher H. Pentland, Catriona Reynolds, Ali Al-Menhali, and Ben Niu. Capillary trapping for geologic carbon dioxide storage ? From pore scale physics to field scale implications. *Int. J. Greenh. Gas Con.*, 40:221–237, sep 2015.
- Ilaria Gimondi and Matteo Salvalaglio. Co2 packing polymorphism under pressure: mechanism and thermodynamics of the i-iii polymorphic transition. *J. Chem. Phys.*, 2017.
- George K. Papadopoulos. Influence of orientational ordering transition on diffusion of carbon dioxide in carbon nanopores. *J. Chem. Phys.*, 114(18):8139–8144, may 2001.
- Th.A Steriotis, K.L Stefanopoulos, N.K Kanellopoulos, A.Ch Mitropoulos, and A. Hoser. The structure of adsorbed CO₂ in carbon nanopores: a neutron diffraction study. *Colloid. Surface. A*, 241(1-3):239–244, jul 2004.
- Yuri B. Melnichenko, H. Mayama, G. Cheng, and T. Blach. Monitoring Phase Behavior of Sub- and Supercritical CO₂ Confined in Porous Fractal Silica with 85% Porosity. *Langmuir*, 26(9):6374–6379, may 2010.

- ²³Gernot Rother, Elizabeth G. Krukowski, Dirk Wallacher, Nico Grimm, Robert J. Bodnar, and David R. Cole. Pore Size Effects on the Sorption of Supercritical CO₂ in Mesoporous CPG-10 Silica. *J. Phys. Chem. C*, 116(1):917–922, jan 2012.
- ²⁴T Sanghi and N R Aluru. Coarse-grained potential models for structural prediction of carbon dioxide (CO₂) in confined environments. *J. Chem. Phys.*, 136(2):024102, jan 2012.
- ²⁵M. Dolores Elola and Javier Rodriguez. Excess Sorption of Supercritical CO₂ within Cylindrical Silica Nanopores. *J. Phys. Chem. C*, 120(2):1262–1269, jan 2016.
- ²⁶Xiaoning Yang and Cuijuan Zhang. Structure and diffusion behavior of dense carbon dioxide fluid in clay-like slit pores by molecular dynamics simulation. *Chem. Phys. Lett.*, 407(4):427–432, 2005.
- ²⁷Alexandru Botan, Benjamin Rotenberg, Virginie Marry, Pierre Turq, and Benot Noetinger. Carbon dioxide in montmorillonite clay hydrates: Thermodynamics, structure, and transport from molecular simulation. *J. Phys. Chem. C*, 114(35):14962–14969, 2010.
- ²⁸Mark E. Tuckerman. *Statistical Mechanics: Theory and Molecular Simulation*. OXFORD UNIVERSITY PRESS, 2010.
- ²⁹Daan Frenkel and Berend Smit. *Understanding Molecular Simulation - From Algorithms to Applications*. ACADEMIC PRESS, 2nd edition, 2002.
- ³⁰Jeremy C. Palmer and Pablo G. Debenedetti. Recent advances in molecular simulation: A chemical engineering perspective. *AIChE J.*, 61(2):370–383, feb 2015.
- ³¹Alessandro Barducci, Giovanni Bussi, and Michele Parrinello. Well-tempered metadynamics: A smoothly converging and tunable free-energy method. *Phys. Rev. Lett.*, 100(2):1–4, 2008.
- ³²Alessandro Barducci, Massimiliano Bonomi, and Michele Parrinello. Metadynamics. *Wires Comput. Mol. Sci.*, 1(5):826–843, sep 2011.
- ³³Omar Valsson, Pratyush Tiwary, and Michele Parrinello. Enhancing Important Fluctuations: Rare Events and Metadynamics from a Conceptual Viewpoint. *Annu. Rev. Phys. Chem.*, 67(1):159–184, may 2016.
- ³⁴Federico Giberti, Matteo Salvalaglio, and Michele Parrinello. Metadynamics studies of crystal nucleation. *IUCrJ*, 2(2):256–266, mar 2015.
- ³⁵J. J. Potoff, J. R. Errington, and A. Z. Panagiotopoulos. Molecular simulation of phase equilibria for mixtures of polar and non-polar components. *Mol. Phys.*, 97(10):1073–1083, nov 1999.
- ³⁶Jeffrey J Potoff and J Ilja Siepmann. Vaporliquid equilibria of mixtures containing alkanes, carbon dioxide, and nitrogen. *AIChE J.*, 47(7):1676–1682, jul 2001.
- ³⁷Giovanni Bussi, Davide Donadio, and Michele Parrinello. Canonical sampling through velocity rescaling. *J. Chem. Phys.*, 126(1):014101, 2007.
- ³⁸Federico Giberti, Matteo Salvalaglio, Marco Mazzotti, and Michele Parrinello. Insight into the nucleation of urea crystals from the melt. *Chem. Eng. Sci.*, 121:51–59, jan 2015.
- ³⁹Matteo Salvalaglio, Thomas Vetter, Federico Giberti, Marco Mazzotti, and Michele Parrinello. Uncovering Molecular Details of Urea Crystal Growth in the Presence of Additives. *J. Am. Chem. Soc.*, 134(41):17221–17233, oct 2012.
- ⁴⁰A Bhattacharyya. No Title. *Bull. Calcutta Math. Soc.*, 35:99–109, 1943.
- ⁴¹Donald G. Truhlar. Valence Bond Theory for Chemical Dynamics. *J. Comput. Chem.*, 28(1):73–86, 2009.
- ⁴²M.J. Abraham, D. van der Spoel, E. Lindahl, B. Hess, and the GROMACS development Team. *GROMACS User Manual version 5.1.1*. www.gromacs.org, 2015.
- ⁴³Gareth A. Tribello, Massimiliano Bonomi, Davide Branduardi, Carlo Camilloni, and Giovanni Bussi. PLUMED 2: New feathers for an old bird. *Comput. Phys. Comm.*, 185(2):604–613, feb 2014.
- ⁴⁴William Humphrey, Andrew Dalke, and Klaus Schulten. VMD – Visual Molecular Dynamics. *J. Mol. Graphics*, 14:33–38, 1996.
- ⁴⁵Aleksey Vishnyakov, Peter I. Ravikovitch, and Alexander V. Neimark. Molecular Level Models for CO₂ Sorption in Nanopores. *Langmuir*, 15(25):8736–8742, dec 1999.

CO₂ packing polymorphism under confinement in cylindrical nanopores: Supplementary Information

Ilaria Gimondi¹ and Matteo Salvalaglio^{1, a)}

Thomas Young Centre and Department of Chemical Engineering, University College London, London WC1E 7JE, UK.

(Dated: 12 November 2018)

Ideal random distribution of relative orientations. All possible relative orientations of two unit vectors in three dimensional space can be mapped in spherical coordinates as a function of the polar angle θ and the azimuthal angle ϕ . Randomly oriented molecules are characterised by a flat probability distribution across all possible orientations. The homogeneous probability density on the surface of a sphere of unit radius has the constant value $p_{rand}(\theta, \phi) = 1/4\pi$, which satisfies the normalization condition:

$$\int_{\theta=0}^{\pi} \int_{\phi=0}^{2\pi} \frac{1}{4\pi} d\phi \sin \theta d\theta = 1 \quad (1)$$

The angle used to map relative orientation between two neighbouring molecules in this work corresponds to the polar angle θ . The probability in θ associated with a random arrangement in spherical coordinates can thus be obtained by integrating out ϕ as follows:

$$P_{ref}(\theta) = \int \int_{\phi=0}^{2\pi} \frac{1}{4\pi} d\phi \sin \theta d\theta = \int \frac{1}{2} \sin \theta d\theta \quad (2)$$

The probability density in θ , in this work used as a fingerprint of the molecular arrangement is then obtained by differentiating $P_{ref}(\theta)$ with respect to θ :

$$p_{ref}(\theta) = \frac{dP_{ref}(\theta)}{d\theta} = \frac{1}{2} \sin \theta \quad (3)$$

One CO₂ molecule. Initially, we perform standard MD runs with only one particle confined in differently sized pores ($d_{pore} = 1, 2, 5, 10$ nm, $l_z = 10$ nm). These simulations last for about 95, 138, 125 and 30 ns, respectively and the potential of the wall is set to the reference $\sigma_{wall} = 0.34$ nm; the initial position of CO₂ is random, but clearly detached from the confinement barrier. This analysis aims at giving an insight into the solely effect of the wall on the motion of a particle when the interaction with other CO₂ is absent.

Figure 1 shows that the single molecule tends to adsorb on the pore, positioning at a distance from the wall that is slightly smaller than the location of the Lennard-Jones well, i.e. $\sigma_{m,C-wall}$ (0.345 nm). Moreover, all the positions along the pore axis are equally likely, and thus the height does not play a major role in the outcome. The

noise in the probability density along z (Figure 1 (a)) is probably due to limited sampling of the area, related to the computational time allowed.

These simulations confirm the strong impact that the pore has on confined CO₂ in the radial direction, in particular the tendency of adsorbing them.

Analysis of the radial distribution of molecules in the pore. We present in Figure 2 the analysis of unbiased MD trajectories, focusing on the position of CO₂ molecule in the radial direction of the pore, for two examples not reported in section 3, namely $r' = 6.847$ (a) and 0.961 (b). In these two cases as well, it is possible to notice that if the pore allows the formation of more layers of molecules or a bulk-like filling, the height of the first peak corresponding to the adsorbed layer decreases with growing density (a); on the other hand, if the pore has no space to accommodate more layers, the height of the peaks increases with ρ_{CO_2} .

WTMetaD set-up. Well-Tempered Metadynamics simulations are performed biasing either λ_I or λ_B . A typical simulation has initial Gaussian height equal to 4 kJ/mol, i.e. ~ 1.5 kT; the width of such Gaussian depends instead on the $r'-\rho_{CO_2}$ conditions, and spans from 3×10^{-4} to 0.6. A biasfactor of 20 is generally employed, but some conditions were explored also with a higher value of this parameter (50).

WTMetaD trajectories. We hereafter present two representative examples of explorative WTMetaD simulations employing λ_I as CV: one in case of liquid conditions (Figure 3 (a), at $r' = 2.075 - \rho_{CO_2} = 8.15$ molecules/nm³), and the other for ordered structures (Figure 3 (b-c), at $r' = 2.075 - \rho_{CO_2} = 12.73$ molecules/nm³). As discussed in section 3, WTMetaD did not enhance the sampling of either ordering phenomena in $r'-\rho_{CO_2}$ conditions identified as liquid from MD or melting events for organized structures; however, some interesting results can be observed. In the case of liquid state, biasing λ_I leads to the creation of an unstable droplet with higher density than the nominal one, that migrates along the z -axis, as shown in Figure 3 (a).

On the other hand, in WTMetaD simulations in ordered areas of the $r'-\rho_{CO_2}$ phase diagram, despite not observing melting, many transitions between ordered structures take place, as reported in Figure 3 (b-c). In these explicative plots, we present a B-C conversion, where B is characterised by low value of λ_I and a 2-peak angle distribution, while C has higher λ_I and a sharp peak on 90° in its angle distribution. Interestingly, it is also possible to notice that during a transition, λ_I changes gradually:

^{a)} Electronic mail: m.salvalaglio@ucl.ac.uk

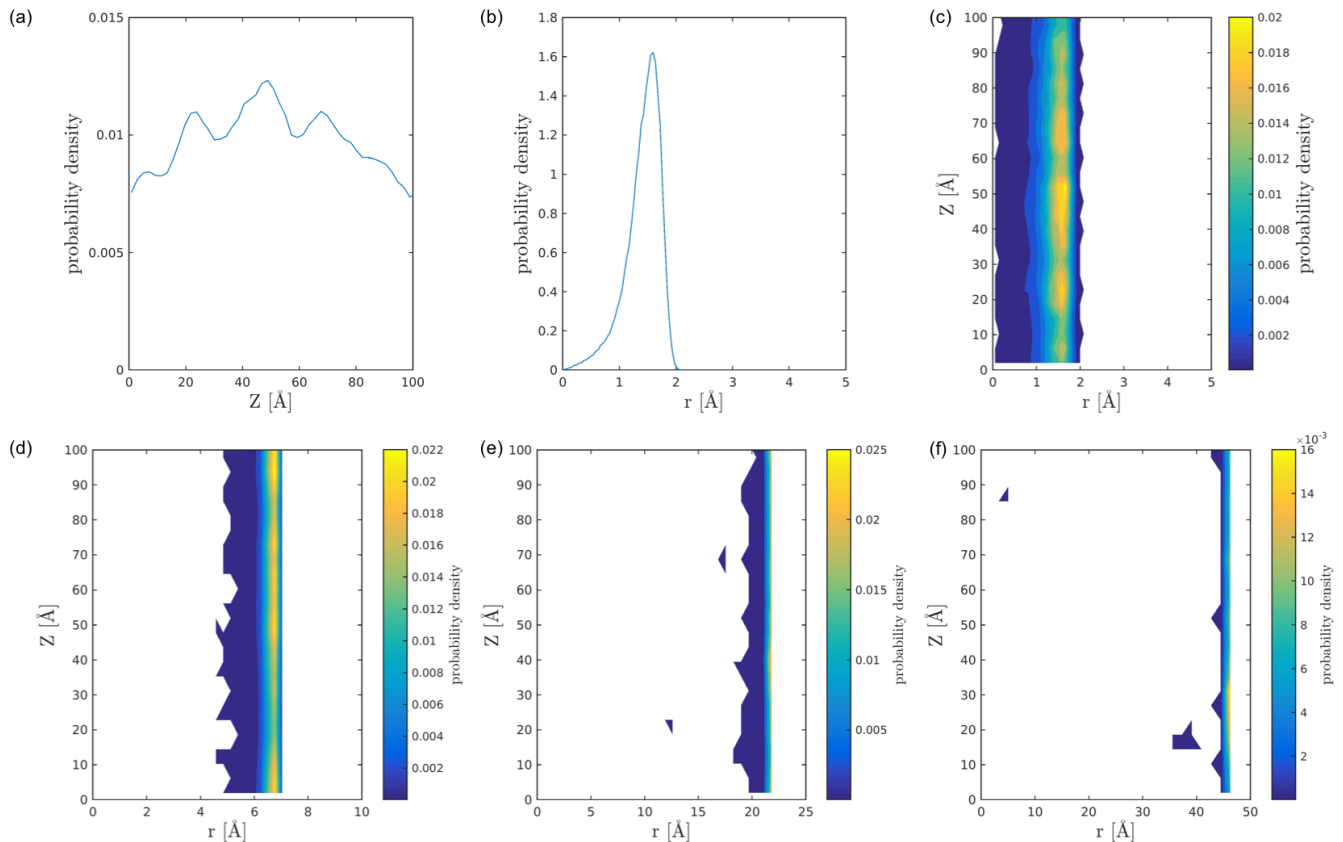


FIG. 1. Probability density of the location of a single CO_2 molecule inside pores with $\sigma_{wall} = 0.34$ nm and diameter 1 nm (a - c), 2 nm (d), 5 nm (e) and 10 nm (f). In (a) and (b) we report the probability density as a function of only the location along the molecular axis, z (a), and of only the radial position, r (b), to better visualise the different role they play: negligible z , while determinant r . In all graphs, the radial position axis ranges from zero, i.e. the pore axis, to the value of the pore radius, reported in \AA .

indeed, as we highlighted in the results, the interconversion between ordered structures generally takes place by progressive rearrangement of unit cells along the z -axis.

Unstable ordered structures. Thanks to both MD and WTMetaD, we identify four stable ordered structures. However, WTMetaD simulations explore a bigger number of configurations that instead are not stable in unbiased simulations, and reorganise in one of the main four. Two significant examples are reported in Figure 4.

The first of these two structures (Figure 4 (a-c)) has CO_2 molecules parallel to each other, aligned along the z -axis, and the density is the same throughout the pore length; the second arrangement presented in Figure 4 (d-f) has well-defined characteristic angles, similar to bulk phase I, as well as a more compact packing than the other phases; such compact packing is achieved by locally increasing the molecular density, which results in areas of the pore with ρ_{CO_2} below the nominal value.

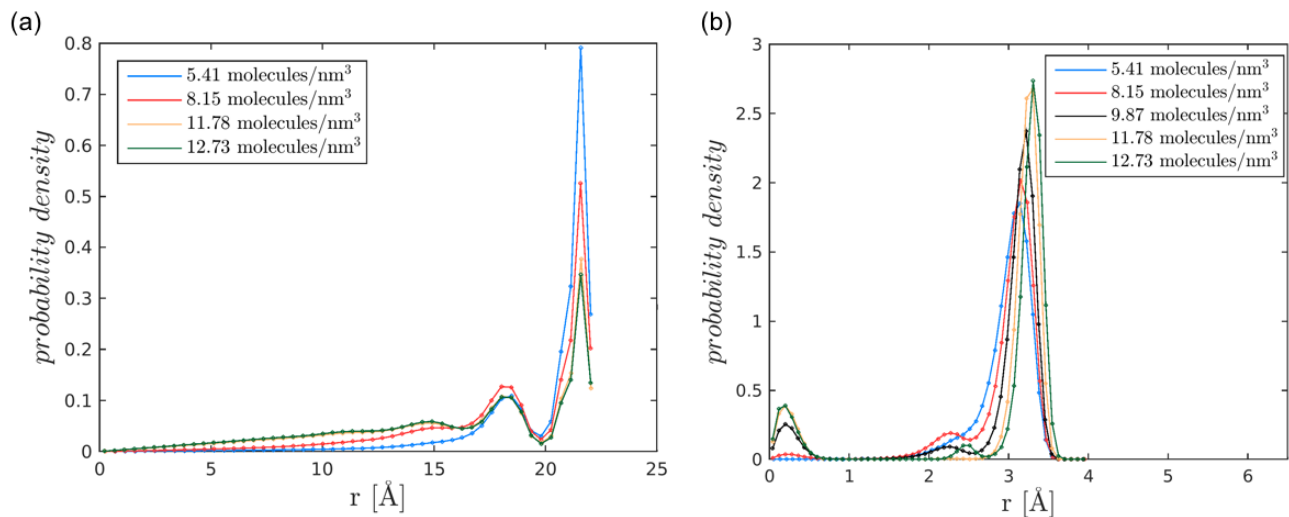


FIG. 2. Probability density profiles of the position of CO₂ molecules in the radial direction of the pore, for the range of densities investigated at different values of r' , namely 6.847 in (a), and 0.961 in (b). Along the pore radius, zero corresponds to the cylinder axis, while the maximum value reported to the radius of the pore.

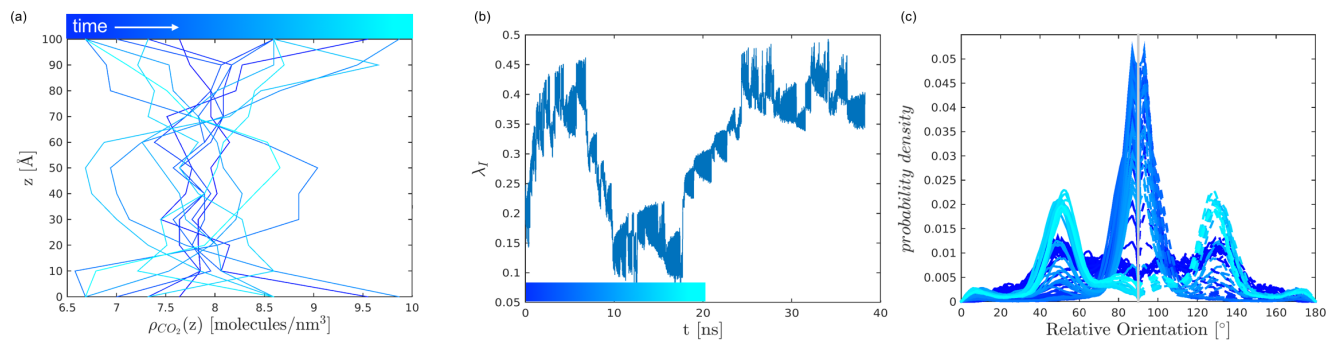


FIG. 3. Explorative WTMetaD biasing λ_I . (a) Axial density profile over time for the creation of a droplet at $r' = 2.075$ - $\rho_{CO_2} = 8.15$ molecules/nm³. (b-c) Time-evolution of the CV λ_I in (b) and of the characteristic angles over the first 20 ns in (c) at $r' = 0.484$ - $\rho_{CO_2} = 12.73$ molecules/nm³. The time scale for the orientation distribution in (c) is highlighted in (b) by dark blue to light blue shades on the time axis.

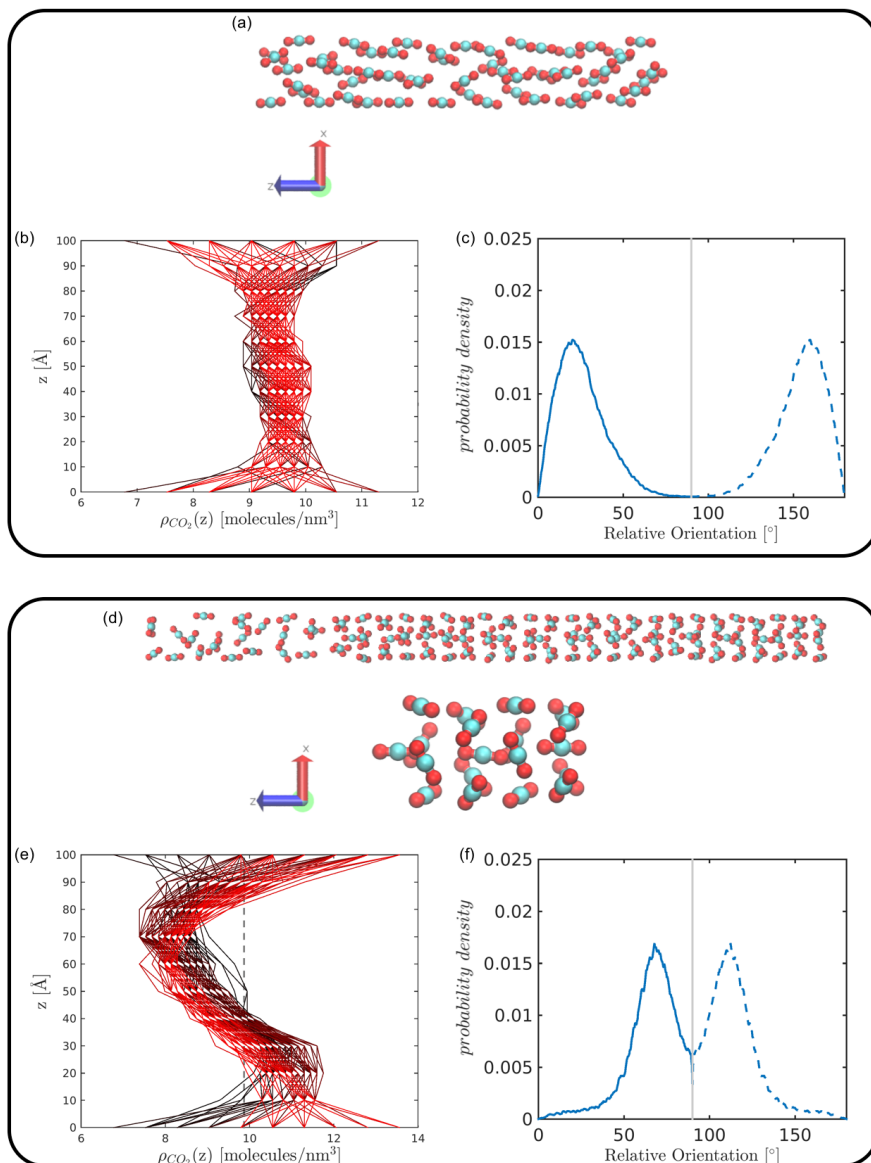


FIG. 4. Examples of unstable ordered structures emerging from WTMetaD with λ_I at $r' = 0.961$ - $\rho_{CO_2} = 9.87$ molecules/nm³. In particular, (a) to (c) report snapshots, density profile in the pore over WTMetaD time (shading from black to red for growing time), and angle distribution for the first arrangement presented; (d) to (f), instead, present the same analysis for the second one.